The Astrophysical Journal, 728:21 (5pp), 2011 February 10 doi:10.1088/0004-637X/728/1/21

EFFECTS OF PHYSICAL FEATURES IN THE SOLAR ATMOSPHERE ON THE CORONAL MASS EJECTION EVOLUTION

Y. Z. Zhang, X. S. Feng, and W. B. Song
SIGMA Weather Group, State Key Laboratory for Space Weather, Center for Space Science and Applied Research, Chinese Academy of Sciences, Beijing 100080, China; yzzhang@spaceweather.ac.cn
Received 2010 February 8; accepted 2010 November 29; published 2011 January 14

ABSTRACT

Based on time-dependent MHD simulation, we investigate how physical features in the solar atmosphere affect the evolution of coronal mass ejections (CMEs). It is found that temperature and density play a crucial role in CME initiation. We argue that lower temperature facilitates the catastrophe's occurrence, and that the CMEs which initiate in low density could gain lower velocity. In our numerical experiment, by employing different values of β, the resulting eruptions of either slow or fast events may be obtained.

Key words: Sun: atmosphere – Sun: coronal mass ejections (CMEs) – Sun: evolution

1. INTRODUCTION

Coronal mass ejections (CMEs) are rapidly evolving, fast-moving heliospheric plasma ejecta originating in the lower solar atmosphere. Both ground- and space-based high-resolution observations can provide comprehensive and homogenous data sets for studies of the CME source region, initiation, and early acceleration and propagation of the CMEs (Schwenn et al. 2006; Gopalswamy et al. 2006; Harrison et al. 2009). A statistical study by Zhang & Dere (2006) shows that a CME usually undergoes a multiphased kinematic evolution, with a rapid increase of CME velocity in the inner corona, followed by a relatively smooth propagation phase in the outer corona. The outward speeds of mass ejection events observed with different instruments vary over a range extending from less than 100 km s^{-1} to greater than 3000 km s^{-1} (Gosling et al. 1976; Hundhausen et al. 1994; Michalek et al. 2009). However, less numerical studies of the relation between the ejection process and the physical features in the solar atmosphere have been reported. It is our purpose here to carry out time-dependent MHD simulations which could determine the physical relationship between the evolution of CMEs and features in the solar atmosphere, such as β, density, and temperature. In so doing, the flux rope erupts from the photospheric surface, which is then regarded as CMEs when the catastrophe occurs during the evolution of the flux rope system. In this paper, the numerical model is described briefly in Section 2, the results are presented in Section 3, and Section 4 concludes this paper with a brief discussion.

2. NUMERICAL MODEL

A catastrophic model is used to investigate the evolution of CMEs (van Tend & Kuperus 1978; Priest & Forbes 1990; Forbes & Isenberg 1991; Isenberg et al. 1993; Forbes & Priest 1995; Hu & Liu 2000; Hu 2001; Hu & Jiang 2001; Hu et al. 2003; Sun & Hu 2005; Ding & Hu 2006; Chen et al. 2006). In general, even if the eruption occurs during this process, magnetic reconnection occurs only in the vertically stretched current sheet since the initial background field is a bipolar configuration. Another highly influential model for solar eruption is the breakout model (Antiochos 1998; Antiochos et al. 1999; DeVore & Antiochos 2008; Lynch et al. 2008) where CMEs occur in multipolar topologies in which reconnection between a sheared arcade and neighboring flux systems triggers the eruption. In this model, reconnection removes the unsheared field above the low-lying, sheared core flux near the neutral line, thereby allowing this core flux that comes into being during this process to burst open. Then, in a three-dimensional system, the mass in the flux rope can drain to the chromosphere as the CME erupts (Titov & Démoulin 1999; Gilbert et al. 2000; Low 2001; Amari et al. 2003; Fan & Gibson 2003, 2004; Gibson et al. 2004; Török & Kliem 2005; Zhou et al. 2006b). This draining could greatly alter the role of mass density in the eruption process.

In our model, the initial background magnetic field is a quadrupolar magnetic field which is the same as the configuration in the breakout model (Antiochos et al. 1999). There exist four topologically disconnected regions: a central arcade astride the equator, a closed bipolar field on each side of the central arcade, and an overlying arcade above them. Although the magnetic configuration considered here has similarities to the breakout model, the process of eruption in our numerical simulation is different from that in the breakout model. Following a similar procedure used by Zhang et al. (2005), we let a flux rope emerge from below the base of the central arcade and enter the arcade in its entirety, and thus we obtain a force-free field solution associated with the flux rope through a time-dependent simulation for our initial state (as seen in Figure 1(a)). After the catastrophe, the flux rope levitates in the solar corona and two current sheets coexist with the rope: a transverse current sheet above and a vertical current sheet below the rope (Figure 1(b)). In particular, magnetic reconnection would take place in both the vertical and the transverse current sheets. It is thus clear that the flux rope is initiated by a purely ideal MHD catastrophe process, and then requires the non-ideal MHD magnetic reconnection process to sustain the acceleration of the eruption. The model is the same as that described in Zhang et al. (2005) and Zhang & Wang (2007).

In this study, we use time-dependent resistive 2.5 dimensional MHD simulations to study the dynamic evolution of a flux rope system in spherical coordinates (r, θ, φ), one may introduce a magnetic flux function $\psi(t, r, \theta)$ related to the magnetic field:

$$\mathbf{B} = \nabla \times \left(\frac{\psi}{r \sin\theta} \hat{\varphi} \right) + B_\varphi \hat{\varphi}, \quad (1)$$

where B_φ is the azimuthal component of the magnetic field. The basic equations are the same as those used in Zhang et al. (2006)

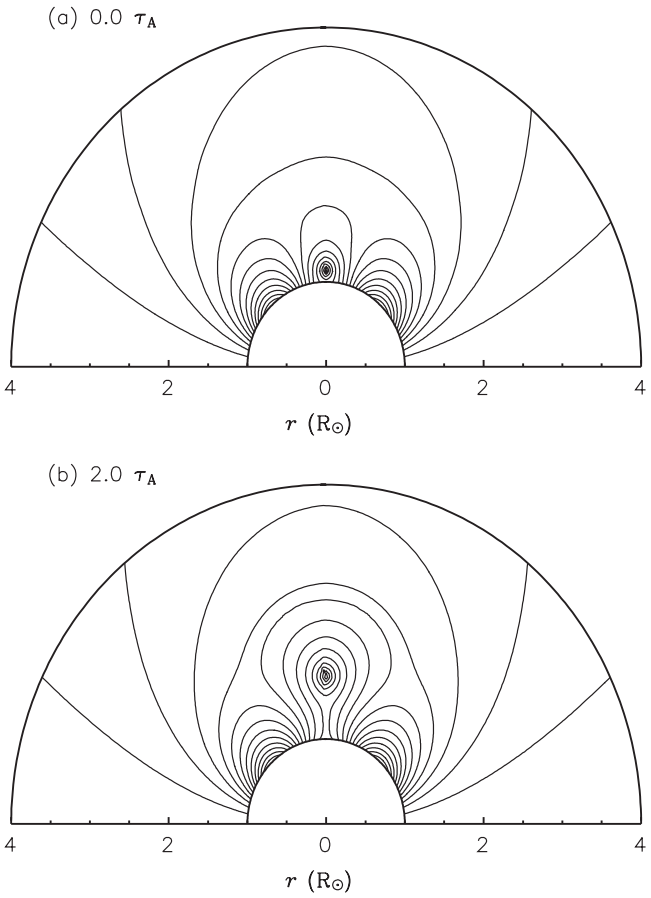

Figure 1. Magnetic configurations of the flux rope system at two separate times: (a) a flux rope that always emerged from below the base of the central arcade in its entirety and (b) the flux rope levitates in the corona and two current sheets coexist with the rope right after a catastrophe.

and are solved with the multistep implicit scheme developed by Hu (1989).

The computational domain is taken to be $1 \leqslant r \leqslant 30$ in units of $R_\odot$ ($R_\odot$ is the solar radius), $0 \leqslant \theta \leqslant \pi/2$, discretized into 130×90 grid points. The grid spacing increases according to a geometric series of common ratio 1.03 from 0.02 at the base ($r = 1$) to 0.86 at the top ($r = 30$), whereas a uniform mesh is adopted in the θ direction. As for the boundary conditions, we use appropriate symmetrical conditions at the pole and equator and calculate the quantities (ρ, v, and T) at the top in terms of equivalent extrapolations, except for B_φ and ψ.

The solar atmosphere is initially assumed to be isothermal, with polytropic index $\gamma = 1.05$ and a ratio of gas to magnetic pressure $\beta = 0.01$. The statement that $\beta = 0.01$ in Cases A, B, and C does not reflect the nonuniformity in the system. Our purpose in stating this is to investigate how the other two essential physical features (temperature and density) affect the evolution of the flux rope system. We then choose different temperatures and densities, and therefore obtain the three cases. At the base, $T = T_0 = 2 \times 10^6$ K and $\rho = \rho_0 = 1.67 \times 10^{-13}$ kg m^{-3} for Case A in Table 1, where T_0 and ρ_0 are taken to be the units for temperature and density, respectively. That leads to a characteristic value of $\psi_0 = (2\mu\rho_0 R T_0 R_\odot^4/\beta)^{1/2} = 5.69 \times 10^{14}$ Wb, taken to be the unit of ψ. Other units of interest are $B_0 = \psi_0/R_\odot^2 = (2\mu\rho_0 R T_0/\beta)^{1/2} = 11.78$ G for field strength, $v_A = B_0/(\mu\rho_0)^{1/2} = (2RT_0/\beta)^{1/2} = 2571$ km s^{-1} for velocity, and $\tau_A = R_\odot/v_A = 271$ s for time. Here, v_A is the characteristic Alfvén speed, $R_\odot$ is the characteristic length, and τ_A is the corresponding characteristic time. In our model, each case has been characterized by temperature, density, and β; it is then possible to compare the magnetic field strengths and speed of the flux rope. We investigate how the different temperatures and densities produce an effect on the speed of the flux rope. In the same way, $T = T_0 = 1 \times 10^6$ K and $\rho = \rho_0 = 3.34 \times 10^{-13}$ kg m^{-3} for Case B and $T = T_0 = 1 \times 10^6$ K and $\rho = \rho_0 = 1.67 \times 10^{-12}$ kg m^{-3} for Case C. Other units for the quantities considered in Cases B and C are shown in Table 1.

Table 1
Units of Temperature, Density, the Ratio of Gas Pressure to Magnetic Pressure, and Other Physical Quantities of Interest in Cases A, B, and C

T (K)	ρ (kg m^{-3})	β	B (G)	ψ (Wb)	v_A (km s^{-1})	τ_A (s)
2×10^6	1.67×10^{-13}	0.01	11.78	5.69×10^{14}	2571	271
1×10^6	3.34×10^{-13}	0.01	11.78	5.69×10^{14}	1818	383
1×10^6	1.67×10^{-12}	0.01	26.34	1.272×10^{15}	1818	383

Note. Here, v_A is the characteristic Alfvén speed.

Table 2
Units of the Ratio of Gas Pressure to Magnetic Pressure and Other Physical Quantities of Interest in Cases A1, A2, A3, and A4

β	B (G)	ψ (Wb)	v_A (km s^{-1})	τ_A (s)
0.008	13.17	6.36×10^{14}	2874	242
0.01	11.78	5.69×10^{14}	2571	271
0.02	8.33	4.023×10^{14}	1818	383
0.05	5.268	2.545×10^{14}	1150	605

Furthermore, we study whether the β of the CME source region has an effect on the eruption of the flux rope system. At the base, β is for the same background temperature and density, such as $T = T_0 = 2 \times 10^6$ K and $\rho = \rho_0 = 1.67 \times 10^{-13}$ kg m^{-3}, where T_0 and ρ_0 are taken to be the units for temperature and density, respectively. As for Case A1, the value of β is 0.008, and other units of interest are $B_0 = 13.17$ G for field strength, $\psi_0 = 6.36 \times 10^{14}$ Wb for ψ, $v_A = 2874$ km s^{-1} for velocity, and $\tau_A = 271$ s for time. While β is 0.01, 0.02, and 0.05, we obtain other three Cases, A2, A3, and A4, respectively. Note that the physical units are listed in Table 2.

Regarding the stored magnetic energy in the corona, Finn & Chen (1990) discussed that magnetic energy increases as the footpoint displacement is increased; Isenberg et al. (1993) showed that the magnetic energy of the flux rope system also increases by transferring magnetic flux from the photosphere to the corona. In our numerical experiment, for convenience, we leap over the evolution of the transition from the photosphere to the corona, and increase the magnetic field inside the flux rope directly. This process is somewhat simple and does not hurt the efforts to understand the catastrophic behavior of the flux rope system. The flux rope is characterized by its poloidal magnetic flux per radian Φ_p and toroidal flux Φ_φ. As we fix the Φ_p and increase the Φ_φ, the flux rope remains attached to the solar surface but expands with increasing Φ_φ at a critical value. The reverse is also true. The two fluxes may be gradually adjusted simply by enhancing B_φ and ψ in the rope, so a new force-free field solution is obtained by the relaxation method.

In all the cases, there exists a catastrophic process in the flux rope system during the early phases. When a current sheet

develops during evolution, numerical resistivity could arise across the current sheet. We have not attempted to estimate the magnitude of the numerical resistivity in the current sheets. In our model, we take special measures to prevent numerical reconnection both in the vertical current sheet and in the transverse current sheet. This treatment was first proposed by Hu et al. (2003) in order to investigate the evolution of flux rope in the framework of ideal MHD. The magnetic flux function ψ along the current sheet is known in advance. At each time step, we check the magnetic flux function ψ on the current sheet and make the ψ along the current sheet invariant during the ideal MHD process. Nevertheless, this special treatment is not employed during the process of resistive MHD in our simulations. As the current sheet builds up, its current density may exceed the threshold to create a microinstability, which would create resistivity and trigger reconnection. Since the vertical and the transverse current sheets reside in the low and high corona, respectively, they should have different critical current densities. Thus, the critical values resulting in the magnetic reconnection are different accordingly. Following Zhang & Wang (2007), we introduce a critical current density for each current sheet, denoted by j_t for the transverse current sheet and j_v for the vertical one, $(j_t, j_v) = (5, 20)$, where $j_0 = B_0/(\mu R_\odot)$, and is taken to be the unit for electric current density. In addition, during the evolution of the catastrophic process the vertical current sheet is strongly subject to the tearing mode instability (Furth et al. 1963). In this experiment, the width of the aspect ratio (length/width) is the unit width. We simply deal with the reconnection process without harming the numerical results. We have used several values for the critical length and obtained almost the same results. We then choose the critical length of the current sheet, $l_c = 0.5\ R_\odot$, as one of the trial values. This length is large enough to satisfy the condition of the tearing mode of instability. Such an expedient measure is somewhat artificial but satisfies our purpose. When the current density near the transverse current sheet exceeds j_t, or that near vertical current sheet exceeds j_v and the length of the vertical current also exceeds l_c, the resistivity of η is set to be 0.01, and η is set to be 0 elsewhere.

Furthermore, the CMEs' onset is due to the flux rope catastrophe in our model; reconnection then occurs in the two current sheets at different reconnection sequences. However, the speed of the flux rope decreases after obtaining its maximum speed in all cases showed. In this study, our primary purpose is to understand the mechanism of CME initiation and acceleration in the inner corona. For simplicity, we assume that the initial corona is isothermal, and with temperature and density in static equilibrium. Thus, we do not physically treat the field-aligned thermal conduction, radiation, and coronal heating, which all play important roles in the energy transformation of the plasma in the solar atmosphere. After accelerating, β in the high corona becomes very high. Thus, the pressure is very high accordingly and holds back the upward motion of the flux rope. For a future study on CME propagation using the same model, we should use a background of solar wind.

3. SIMULATION RESULTS

As mentioned in the previous section, we intend to discuss the numerical results. Our catastrophic flux rope model is a storage model. It is different from the flux injection model which has been proposed by Chen (1989). In our numerical simulation, the emerging process is a storage process. When energy storage reaches a critical point, catastrophe occurs. The

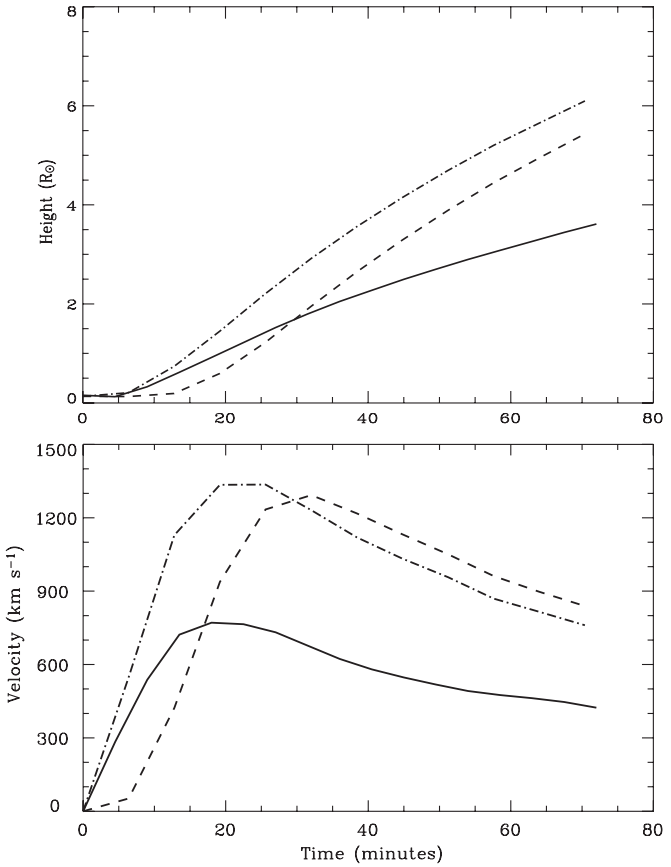

Figure 2. Height and velocity of the flux rope axis vs. time for all of the three cases, A (solid), B (dashed), and C (dot-dashed), in the upper panel and lower panel, respectively.

magnetic properties of the flux rope are represented by its poloidal magnetic flux per radian Φ_p and toroidal flux Φ_φ. In this experiment, calculations are carried out for the different values of Φ_φ with a fixed Φ_p. One value of Φ_p is chosen, 0.6 in units of ψ_0, for all three Cases A, B, and C. It is found that for the value of Φ_p, the flux rope system exhibits a catastrophic behavior with respect to a gradual increase of Φ_φ. For Case A, the catastrophic point lies between $\Phi_\varphi = 0.0415$ and 0.0416, and we find that the catastrophic points for Cases B and C lie between $\Phi_\varphi = 0.0399$ and 0.0400, respectively. It can be seen from this that the catastrophe occurs simultaneously in Cases B and C, which is due to the same background temperature of both cases. Moreover, owing to the higher temperature, the value of the catastrophic point of Case A is larger than that of the other two cases. This indicates that the temperature could determine the dynamics of catastrophe during the evolution of the flux rope. It shows that the flux rope erupts more easily when the temperature is much lower.

We use two parameters to characterize the evolution of the flux rope system eruption: h_a, the height of the rope axis, and v_a, the velocity of the rope axis. Figure 2 shows h_a and v_a as a function of time for the three cases, A, B, and C. Following a similar procedure used by Zhang & Wang (2007), we increase the Φ_φ of the flux rope from 0.0400, 0.0360, and 0.0360 to 0.0416, 0.0400, and 0.0400, respectively. In all the three cases, the flux rope starts erupting just after catastrophe occurs. Then, magnetic reconnection occurs in the two current sheets after. In the lower panel, for Case A, v_a is increased at about $t = 9$ minutes after the catastrophe has just occurred. Reconnection

occurs in the transverse current sheet at about $t = 13$ minutes and in the vertical current sheet at about $t = 18$ minutes. v_a attains a maximum speed of 779.1 km s^{-1} at about $t = 22$ minutes. For both Cases B and C, the flux rope is immediately accelerated without initial slow rising phases. For Case B, reconnection sets in simultaneously in the two current sheets at about $t = 25$ minutes, and then v_a reaches its maximum speed of 1293 km s^{-1} at about $t = 32$ minutes. Similarly, for Case C, reconnection sets in simultaneously in the two current sheets at about $t = 19$ minutes, and then v_a attains a maximum speed of 1336 km s^{-1} at about $t = 25$ minutes. Obviously, the speed of the erupted flux rope in Case A is much lower than that in the other two cases. In the source region with lower temperature, both the current sheet length and the current density increase rapidly, and reconnection occurs in the current sheet rapidly. Due to the different temperatures of the source region in Case A and in the other two cases, the reconnection sequence during the erupting process is different. The reconnection that happens first in the transverse current sheet and later in the vertical one in Case A is apt to produce a gradual acceleration of the flux rope, and the reconnection starting simultaneously in the two current sheets in Cases B and C leads to an impulsive acceleration of the flux rope. We argue that the reconnection sequence plays a critical role in the motion of the erupting flux rope after the catastrophe. In the upper panel, for all three cases, the flux rope usually undergoes a main acceleration phase characterized by a rapid increase of CME velocity under 2 $R_\odot$. Therefore, we consider the CMEs to be initiated by the catastrophe of the flux rope, and then accelerated by reconnection in the two current sheets in the inner corona. With the same background temperature, the maximum speed of CMEs which erupt from the region of higher density could be obtained earlier and a little faster than those which initiate from the region of lower density. Furthermore, our results show that the speed of CMEs, which initiate from the source region with lower temperature and higher density, is recognized to be much faster than that from other source regions.

Figure 3 shows h_a and v_a as a function of time for the four cases, A1, A2, A3, and A4. For all the four cases, the flux rope erupts just after the catastrophe occurs, and then magnetic reconnection first occurs in the transverse current sheet and later in the vertical one. As can be seen in the lower panel, v_a attains a maximum speed of 1068 km s^{-1} at about $t = 24$ minutes for Case A1, 779.1 km s^{-1} at about $t = 22$ minutes for Case A2, 437.4 km s^{-1} at about $t = 45$ minutes for Case A3, and 384.5 km s^{-1} at about $t = 70$ minutes for Case A4. In Table 2, we list the strength of the magnetic field in each of the four cases. When the value of β becomes increasingly large, the relevant strength of the magnetic field gets weaker and weaker, and the corresponding maximum speed of CMEs becomes slower. It was found that a smooth transition from slow to fast eruptions occurs when decreasing the ratio of gas pressure to magnetic pressure. This suggests that the slow and fast CMEs could have identical driving mechanisms (e.g., Chen et al. 2007). In the upper panel, for all the four cases, CMEs generally undergo a main acceleration phase characterized by a rapid increase of CME velocity under 2 $R_\odot$. Further discussion will be presented at the end of the following paragraph.

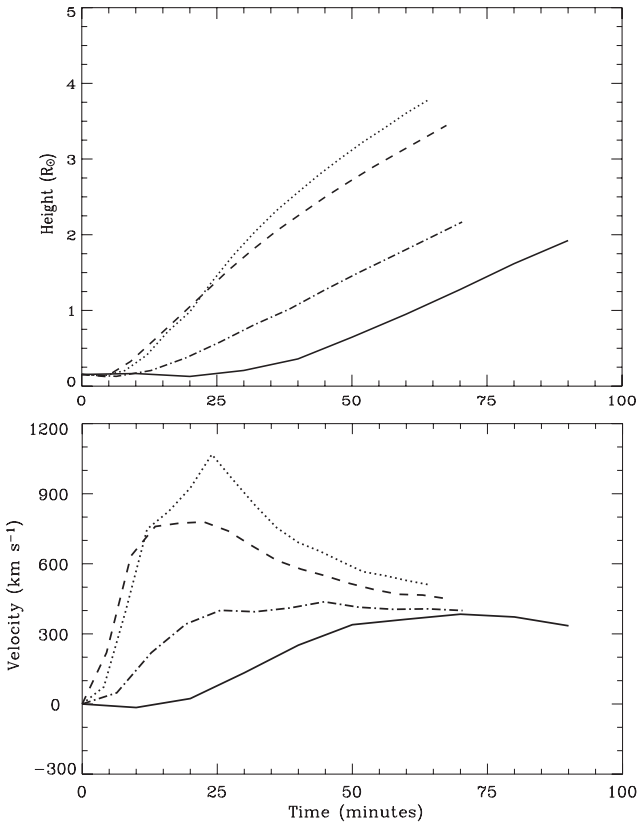

Figure 3. Height and velocity of the flux rope axis vs. time for all of the four cases, A1 (dotted), A2 (dashed), A3 (dot-dashed), and A4 (solid), in the upper panel and lower panel, respectively.

4. DISCUSSION

CMEs are large-scale eruptive phenomena that favor complex magnetic configurations and multiple flux systems (e.g., Wang et al. 2006; Zhou et al. 2006a). The physical features in the solar atmosphere, such as β, temperature, and density, determine the process of CMEs. In our model, the flux rope is embedded in a quadrupole magnetic field and its eruption is initiated by a catastrophic process and then requires magnetic reconnection to sustain the acceleration of the eruption (Zhang & Wang 2007). In this study, we use the catastrophic flux rope model to investigate the relations between the physical properties and the evolution of CMEs, and find that the evolution of the flux rope depends on the physical features of the initiation region in the solar atmosphere.

The main conclusion from our numerical experiment is that temperature and density in the solar atmosphere play determining roles in CMEs' initiation. Using our model, we argue that temperature determines the catastrophic process of the flux rope system, i.e., the lower temperature facilitates the catastrophic occurrence. With the same background temperature, CMEs which erupt from the region of higher density will be much faster than which initiate from the region of lower density. Moreover, it was found that CMEs which initiate from the source region with lower temperature and higher density are found to be much faster than CMEs from other source regions.

Previously, Sheeley et al. (1999) separated CMEs into two classes: (1) gradual CMEs, which are associated with erupting prominences and have speeds in the range of 400–600 km s^{-1}, and (2) impulsive CMEs, which are often associated with flares and have speeds typically in excess of 750 km s^{-1}. They come from different magnetic regions on the Sun: fast CMEs come from active regions, while slow CMEs come from filament channels outside active regions. Later, Subramanian & Dere (2001) surveyed 32 CMEs during 1996 January to 1998 June whose source regions are well observed on the solar disk in EIT 195 Å images. They found that 13 (41%) of these

events are associated with active regions without prominence eruptions, 14 (44%) are associated with eruptions of active region prominences, and 5 (15%) are associated with eruptions of prominences outside active regions. With regard to the locations of CME source regions, Zhou et al. (2003) found that about 79% of CMEs initiate from active regions and only 21% originate outside active regions. However, Zhang & Dere (2006) showed the observed properties of the 50 CME events selected in order of observation date, and found that the statistical distributions of CME acceleration, both magnitude and duration, have a wide distribution that presents a continuous spectrum of CME events, ranging from extremely gradual ones all the way to the extremely impulsive ones. Therefore, it is worth noting that the speed distribution of CME represents a continuous spectrum (Low & Zhang 2002). Yurchyshyn et al. (2005) presented the fact that the two groups of CMEs can be modeled by a single distribution which may suggest that the same driving mechanism is acting in both slow and fast dynamical types of CMEs (e.g., Chen et al. 2007). Our numerical experiment employs different values of β, and the resulting eruption may yield either slow or fast events. The convincing cases that the continuum of CME speed is attributable to source-region temperature and magnetic field need to do some statistical study on CMEs which are driven from different source regions (e.g., active region, filament, etc). As a rule, CMEs undergo a main acceleration phase characterized by a rapid increase of CME velocity under 2 $R_{\odot}$. Though in our simulation we did not consider the solar wind, which did not affect the process of the onset and acceleration of the flux rope, for future studies of CME propagation using the same model, we should use a solar wind background.

The authors are greatly indebted to the anonymous referee for helpful comments and suggestions. One of the authors (Y.Z.Z.) thanks Professor Y. Q. Hu for his valuable suggestions and Professor J. X. Wang for useful discussions. The work is jointly supported by the National Natural Science Foundation of China (41031066, 40921063, 40874091, 40890162, 40904050, 40874077, and 40536029), and the Specialized Research Fund for State Key Laboratories. The numerical calculation has been completed on our SIGMA Cluster computing system.

REFERENCES

Amari, T., Luciani, J. F., Aly, J. J., Mikic, Z., & Linker, J. 2003, ApJ, 595, 1231
Antiochos, S. K. 1998, ApJ, 502, L181
Antiochos, S. K., DeVore, C. R., & Klimchuk, J. A. 1999, ApJ, 510, 485
Chen, J. 1989, ApJ, 338, 453
Chen, Y., Chen, X. H., & Hu, Y. Q. 2006, ApJ, 644, 587
Chen, Y., Hu, Y. Q., & Sun, S. J. 2007, ApJ, 665, 1421
DeVore, C. R., & Antiochos, S. K. 2008, ApJ, 680, 740
Ding, J. Y., & Hu, Y. Q. 2006, Sol. Phys., 233, 45
Fan, Y., & Gibson, S. E. 2003, ApJ, 589, L105
Fan, Y., & Gibson, S. E. 2004, ApJ, 609, 1123
Finn, J. M., & Chen, J. 1990, ApJ, 349, 345
Forbes, T. G., & Isenberg, P. A. 1991, ApJ, 373, 294
Forbes, T. G., & Priest, E. R. 1995, ApJ, 446, 377
Furth, H. P., Killeen, J., & Rosenbluth, M. N. 1963, Phys. Fluids, 6, 459
Gibson, S. E., Fan, Y., Mandrini, C., Fisher, G., & Démoulin, P. 2004, ApJ, 617, 600
Gilbert, H. R., Holzer, T. E., Burkepile, J. T., & Hundhausen, A. J. 2000, ApJ, 537, 503
Gopalswamy, N., Mikic, Z., Maia, D., Alexander, D., Cremades, H., Kaufmann, P., Tripathi, D., & Wang, Y.-M. 2006, Space Sci. Rev., 123, 303
Gosling, J. T., Hildner, E., MacQueen, R. M., Munro, R. H., Poland, A. I., & Ross, C. L. 1976, Sol. Phys., 48, 389
Harrison, R. A., Davis, C. J., & Davies, J. A. 2009, Sol. Phys., 259, 277
Hu, Y. Q. 1989, J. Comput. Phys., 84, 441
Hu, Y. Q. 2001, Sol. Phys., 200, 115
Hu, Y. Q., & Jiang, Y. W. 2001, Sol. Phys., 203, 309
Hu, Y. Q., Li, G. Q., & Xing, X. Y. 2003, J. Geophys. Res., 108, 1072
Hu, Y. Q., & Liu, W. 2000, ApJ, 540, 1119
Hundhausen, A. J., Burkepile, J. T., & St. Cyr, O. C. 1994, J. Geophys. Res., 99, 6543
Isenberg, P. A., Forbes, T. G., & Démoulin, P. 1993, ApJ, 417, 368
Low, B. C. 2001, J. Geophys. Res., 106, 25141
Low, B. C., & Zhang, M. 2002, ApJ, 564, L53
Lynch, B. J., Antiochos, S. K., DeVore, C. R., Luhmann, J. G., & Zurbuchen, T. H. 2008, ApJ, 683, 1192
Michalek, G., Gopalswamy, N., & Yashiro, S. 2009, Sol. Phys., 260, 401
Priest, E. R., & Forbes, T. G. 1990, Sol. Phys., 126, 319
Schwenn, R., et al. 2006, Space Sci. Rev., 123, 127
Sheeley, N. R., Walters, J. H., Wang, Y.-M., & Howard, R. A. 1999, J. Geophys. Res., 104, 24739
Subramanian, P., & Dere, K. P. 2001, ApJ, 561, 372
Sun, S. J., & Hu, Y. Q. 2005, J. Geophys. Res., 110, 05102
Titov, V. S., & Démoulin, P. 1999, A&A, 351, 707
Török, T., & Kliem, B. 2005, ApJ, 630, L97
van Tend, W., & Kuperus, M. 1978, Sol. Phys., 59, 115
Wang, J. X., Zhou, G. P., Wen, Y. Y., Zhang, Y. Z., Wang, H. N., Deng, Y. Y., Zhang, J., & Harra, L. K. 2006, ChJA&A, 6, 247
Yurchyshyn, V., Yashiro, S., Abramenko, V., Wang, H., & Gopalswamy, N. 2005, ApJ, 619, 599
Zhang, J., & Dere, K. P. 2006, ApJ, 649, 1100
Zhang, Y. Z., Hu, Y. Q., & Wang, J. X. 2005, ApJ, 626, 1096
Zhang, Y. Z., & Wang, J. X. 2007, ApJ, 663, 592
Zhang, Y. Z., Wang, J. X., & Hu, Y. Q. 2006, ApJ, 641, 572
Zhou, G. P., Wang, J. X., & Cao, Z. L. 2003, A&A, 397, 1057
Zhou, G. P., Wang, J. X., & Zhang, J. 2006a, A&A, 445, 1133
Zhou, G. P., Wang, J. X., Zhang, J., Chen, P. F., Ji, H. S., & Dere, K. 2006b, ApJ, 651, 1238